

Measurement of the branching ratios for the decays of D_s^+ to $\eta\pi^+$, $\eta'\pi^+$, $\eta\rho^+$, and $\eta'\rho^+$

C. P. Jessop, K. Lingel, H. Marsiske, M. L. Perl, S. F. Schaffner, D. Ugolini, R. Wang, and X. Zhou
Stanford Linear Accelerator Center, Stanford University, Stanford, California 94309

T. E. Coan, V. Fadeyev, I. Korolkov, Y. Maravin, I. Narsky, V. Shelkov, J. Staeck, R. Stroynowski, I. Volobouev,
 and J. Ye
Southern Methodist University, Dallas, Texas 75275

M. Artuso, A. Efimov, F. Frasconi, M. Gao, M. Goldberg, D. He, S. Kopp, G. C. Moneti, R. Mountain, Y. Mukhin,
 S. Schuh, T. Skwarnicki, S. Stone, G. Viehhauser, and X. Xing
Syracuse University, Syracuse, New York 13244

J. Bartelt, S. E. Csorna, V. Jain, and S. Marka
Vanderbilt University, Nashville, Tennessee 37235

A. Freyberger, R. Godang, K. Kinoshita, I. C. Lai, P. Pomianowski, and S. Schrenk
Virginia Polytechnic Institute and State University, Blacksburg, Virginia 24061

G. Bonvicini, D. Cinabro, R. Greene, and L. P. Perera
Wayne State University, Detroit, Michigan 48202

B. Barish, M. Chadha, S. Chan, G. Eigen, J. S. Miller, C. O'Grady, M. Schmidtler, J. Urheim, A. J. Weinstein,
 and F. Würthwein
California Institute of Technology, Pasadena, California 91125

D. M. Asner, D. W. Bliss, W. S. Brower, G. Masek, H. P. Paar, and V. Sharma
University of California, San Diego, La Jolla, California 92093

J. Gronberg, R. Kutschke, D. J. Lange, S. Menary, R. J. Morrison, H. N. Nelson, T. K. Nelson, C. Qiao, J. D. Richman,
 D. Roberts, A. Ryd, and M. S. Witherell
University of California, Santa Barbara, California 93106

R. Balest, B. H. Behrens, K. Cho, W. T. Ford, H. Park, P. Rankin, J. Roy, and J. G. Smith
University of Colorado, Boulder, Colorado 80309-0390

J. P. Alexander, C. Bebek, B. E. Berger, K. Berkelman, K. Bloom, D. G. Cassel, H. A. Cho, D. M. Coffman,
 D. S. Crowcroft, M. Dickson, P. S. Drell, K. M. Ecklund, R. Ehrlich, R. Elia, A. D. Foland, P. Gaidarev, B. Gittelman,
 S. W. Gray, D. L. Hartill, B. K. Heltsley, P. I. Hopman, J. Kandaswamy, N. Katayama, P. C. Kim, D. L. Kreinick,
 T. Lee, Y. Liu, G. S. Ludwig, J. Masui, J. Mevissen, N. B. Mistry, C. R. Ng, E. Nordberg, M. Ogg,* J. R. Patterson,
 D. Peterson, D. Riley, A. Soffer, and C. Ward
Cornell University, Ithaca, New York 14853

M. Athanas, P. Avery, C. D. Jones, M. Lohner, C. Prescott, S. Yang, J. Yelton, and J. Zheng
University of Florida, Gainesville, Florida 32611

G. Brandenburg, R. A. Briere, Y. S. Gao, D. Y.-J. Kim, R. Wilson, and H. Yamamoto
Harvard University, Cambridge, Massachusetts 02138

T. E. Browder, F. Li, Y. Li, and J. L. Rodriguez
University of Hawaii at Manoa, Honolulu, Hawaii 96822

T. Bergfeld, B. I. Eisenstein, J. Ernst, G. E. Gladding, G. D. Gollin, R. M. Hans, E. Johnson, I. Karliner, M. A. Marsh,
 M. Palmer, M. Selen, and J. J. Thaler
University of Illinois, Urbana-Champaign, Illinois 61801

K. W. Edwards
*Carleton University, Ottawa, Ontario, Canada K1S 5B6
 and the Institute of Particle Physics, Canada*

A. Bellerive, R. Janicek, D. B. MacFarlane, K. W. McLean, and P. M. Patel
McGill University, Montréal, Québec, Canada H3A 2T8
and the Institute of Particle Physics, Canada

A. J. Sadoff
Ithaca College, Ithaca, New York 14850

R. Ammar, P. Baringer, A. Bean, D. Besson, D. Coppage, C. Darling, R. Davis, N. Hancock, S. Kotov, I. Kravchenko,
 and N. Kwak
University of Kansas, Lawrence, Kansas 66045

S. Anderson, Y. Kubota, M. Lattery, J. J. O'Neill, S. Patton, R. Poling, T. Riehle, V. Savinov, and A. Smith
University of Minnesota, Minneapolis, Minnesota 55455

M. S. Alam, S. B. Athar, Z. Ling, A. H. Mahmood, H. Severini, S. Timm, and F. Wappler
State University of New York at Albany, Albany, New York 12222

A. Anastassov, S. Blinov,[†] J. E. Duboscq, K. D. Fisher, D. Fujino,[‡] R. Fulton, K. K. Gan, T. Hart, K. Honscheid,
 H. Kagan, R. Kass, J. Lee, M. B. Spencer, M. Sung, A. Undrus,[†] R. Wanke, A. Wolf, and M. M. Zoeller
Ohio State University, Columbus, Ohio 43210

B. Nemati, S. J. Richichi, W. R. Ross, P. Skubic, and M. Wood
University of Oklahoma, Norman, Oklahoma 73019

M. Bishai, J. Fast, E. Gerndt, J. W. Hinson, N. Menon, D. H. Miller, E. I. Shibata, I. P. J. Shipsey, and M. Yurko
Purdue University, West Lafayette, Indiana 47907

L. Gibbons, S. D. Johnson, Y. Kwon, S. Roberts, and E. H. Thorndike
University of Rochester, Rochester, New York 14627

(CLEO Collaboration)

(Received 31 December 1997; published 29 July 1998)

Using a data sample with an integrated luminosity of 3.9 fb^{-1} collected in e^+e^- annihilation with the CLEO-II detector at the Cornell Electron Storage Ring, we have measured the branching ratios for the decay modes $D_s^+ \rightarrow (\eta, \eta') \pi^+$ and $D_s^+ \rightarrow (\eta, \eta') \rho^+$ relative to $D_s^+ \rightarrow \phi \pi^+$. These decay modes are among the most common hadronic decays of the D_s^+ , and can be related by factorization to the semileptonic decays $D_s^+ \rightarrow (\eta, \eta') \ell^+ \nu_l$. The results obtained are compared with previous CLEO results and with the branching ratios measured for the related semileptonic decays. We also report results on the Cabibbo-suppressed decays of the D^+ to the same final states. [S0556-2821(98)00417-2]

PACS number(s): 13.20.Fc, 13.65.+i, 14.40.Lb

I. INTRODUCTION

Among the most common hadronic decay modes for the D_s^+ are the decays $D_s^+ \rightarrow (\eta, \eta') \pi^+$ and $D_s^+ \rightarrow (\eta, \eta') \rho^+$, where the notation $D_s^+ \rightarrow (\eta, \eta') \pi^+$ represents the decays $D_s^+ \rightarrow \eta \pi^+$ and $D_s^+ \rightarrow \eta' \pi^+$. As can be seen from Fig. 1, they are related by factorization to the semileptonic decays $D_s^+ \rightarrow (\eta, \eta') \ell^+ \nu_l$. This relation has been extensively discussed by Kamal, Xu, and Czarnecki [1]. One prediction of the factorization hypothesis is that the D_s^+ decay rate to $\eta \rho^+$

can be simply related to the corresponding semileptonic decay rate evaluated at $q^2 = m_\rho^2$:

$$\Gamma(D_s^+ \rightarrow \eta \rho^+) = 6 \pi^2 a_1^2 f_\rho^2 |V_{ud}|^2 \times \frac{d\Gamma}{dq^2}(D_s^+ \rightarrow \eta \ell^+ \nu_l)|_{(q^2=m_\rho^2)}. \quad (1)$$

Here f_ρ is the decay constant for the ρ and a_1 is a strong interaction coefficient that is measured in two-body hadronic D^0 decays.

To test this factorization prediction experimentally, a shape for the form factor must be assumed. It is expected to be very close to the form factor for $D^0 \rightarrow K^- e^+ \nu_e$, for which

*Permanent address: University of Texas, Austin, TX 78712.

[†]Permanent address: BINP, RU-630090 Novosibirsk, Russia.

[‡]Permanent address: Lawrence Livermore National Laboratory, Livermore, CA 94551.

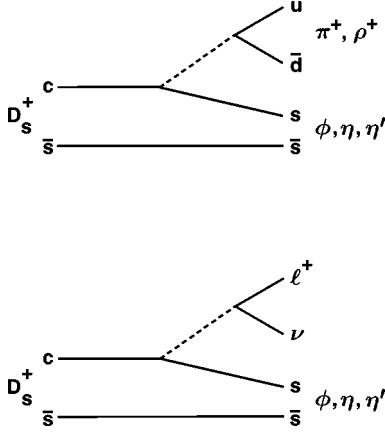


FIG. 1. Related Feynman diagrams for hadronic and semileptonic D_s^+ decays.

$$\left. \frac{\Gamma(D^0 \rightarrow K^- e^+ \nu_e)}{d\Gamma(D^0 \rightarrow K^- e^+ \nu_e)/dq^2} \right|_{(q^2=m_\rho^2)} = 1.30 \pm 0.01 \text{ GeV}^2.$$

This number is calculated using the CLEO measurement of the form factor [2]. Assuming a similar pole shape for the D_s^+ form factor yields the prediction $\Gamma(D_s^+ \rightarrow \eta \rho^+)/\Gamma(D_s^+ \rightarrow \eta e^+ \nu_e) \approx 2.9$ and $\Gamma(D_s^+ \rightarrow \eta' \rho^+)/\Gamma(D_s^+ \rightarrow \eta' e^+ \nu_e) \approx 2.9$ [3].

In 1992 CLEO [4] measured the branching ratios for the hadronic modes studied here using a much smaller data sample of 0.69 fb^{-1} . Combining these measurements with the more recent CLEO measurements of the semileptonic modes [7], we calculate the $\Gamma(D_s^+ \rightarrow \eta \rho^+)/\Gamma(D_s^+ \rightarrow \eta e^+ \nu_e) = 4.3 \pm 1.1$ and $\Gamma(D_s^+ \rightarrow \eta' \rho^+)/\Gamma(D_s^+ \rightarrow \eta' e^+ \nu_e) = 14.8 \pm 5.8$. The last number is well above the factorization prediction of 2.9. Models that modify the factorization picture to include final state interactions are able to fit experimental measurements for a long list of charm decay modes. Even those models, however, cannot account for the very large branching ratio for $D_s^+ \rightarrow \eta' \rho^+$ [5,6]; there appears to be no other mode that can rescatter to this mode in sufficient quantity to produce such a large branching ratio.

Because of the interest in these branching fractions, we have remeasured them using the much larger data sample now available. In the present analysis we use data corresponding to an integrated luminosity of 3.9 fb^{-1} (which includes the 0.69 fb^{-1} used in the previous analysis) to remeasure the four modes, $D_s^+ \rightarrow (\eta, \eta') \pi^+$ and $D_s^+ \rightarrow (\eta, \eta') \rho^+$. The data were collected with the CLEO II detector at the Cornell Electron Storage Ring (CESR), at center-of-mass energies equal to the mass of the $Y(4S)$ and in the continuum just below the $Y(4S)$ resonance.

The CLEO-II detector is designed to detect both charged and neutral particles with high resolution and efficiency. The detector consists of a charged-particle tracking system surrounded by a time-of-flight scintillator system. These are in turn surrounded by an electromagnetic calorimeter which consists of 7800 thallium-doped CsI crystals. This inner detector is immersed in a 1.5 T solenoidal magnetic field generated by a superconducting coil. Muon detection is achieved

using proportional tubes interleaved with iron. A more complete description of the detector can be found elsewhere [8].

II. EVENT SELECTION

All events in this analysis are required to pass standard CLEO criteria for hadronic events. Since all the signal modes involve only pions in the final state, systematic errors are reduced by imposing no hadron identification cuts on either signal modes or the normalization mode. All D_s^+ candidates are required to have $x = P_{D_s}/P_{max} > 0.63$ ($P_{max}^2 = E_{beam}^2 - M_{D_s}^2$) to suppress combinatoric background. Throughout this paper, reference to a particular charge state implies the inclusion of the charge-conjugate state as well.

All photons are required to be in the good barrel region of the calorimeter ($|\cos \theta| < 0.71$), to have a minimum energy of 30 MeV, and to not match the projection of a charged track. We choose pairs of photons whose invariant mass is within $2.5 \sigma(M)$ of the nominal π^0 mass; $\sigma(M)$ is approximately $6 \text{ MeV}/c^2$. We then kinematically constrain the $\gamma\gamma$ pairs to the nominal π^0 mass in order to improve the momentum resolution of the π^0 . We also require that $|\cos \theta_{\pi^0}| < 0.8$, where θ_{π^0} is the angle between one γ in the π^0 rest frame and the π^0 momentum in the laboratory frame. The signal is flat in $\cos \theta_{\pi^0}$ and the background peaks toward $\cos \theta_{\pi^0} = +1$.

For $\eta \rightarrow \gamma\gamma$ decays, the η is selected in a manner similar to the π^0 , but with the additional constraint that photons which could be paired to make π^0 's with momentum greater than $0.8 \text{ GeV}/c$ are rejected. We also detect η 's using the $\eta \rightarrow \pi^+ \pi^- \pi^0$ decay chain, although this mode gives a sample with fewer events and less significance than the two-photon decay mode. A π^0 momentum greater than $0.4 \text{ GeV}/c$ is required. All η candidates within $2.5 \sigma(M)$ of the nominal mass are considered, where $\sigma(M)$ is the rms mass resolution for the given mode, typically about $14 \text{ MeV}/c^2$ for the $\gamma\gamma$ mode and $6 \text{ MeV}/c^2$ for the $\pi^+ \pi^- \pi^0$ mode. In order to improve the momentum resolution of the η , the decay particles from the η are kinematically constrained to the nominal η mass.

To select η' candidates we use the $\eta \pi^+ \pi^-$ final state, where the η is detected in both $\gamma\gamma$ and $\pi^+ \pi^- \pi^0$ modes. Both η and η' candidates are kinematically constrained to the nominal mass in order to improve the momentum resolution.

Reconstruction efficiencies and invariant mass resolutions were determined by using a GEANT-based [9] Monte Carlo (MC) simulation of the detector.

III. D_s^+ DECAYS INTO MODES CONTAINING A π^+

Five modes are studied in which a pion is produced in the weak decay:

- (1) $D_s^+ \rightarrow \phi \pi^+$ (the normalization mode), $\phi \rightarrow K^+ K^-$
- (2) $D_s^+ \rightarrow \eta \pi^+$, $\eta \rightarrow \gamma\gamma$
- (3) $D_s^+ \rightarrow \eta \pi^+$, $\eta \rightarrow \pi^+ \pi^- \pi^0$
- (4) $D_s^+ \rightarrow \eta' \pi^+$, $\eta' \rightarrow \eta \pi^+ \pi^-$, $\eta \rightarrow \gamma\gamma$

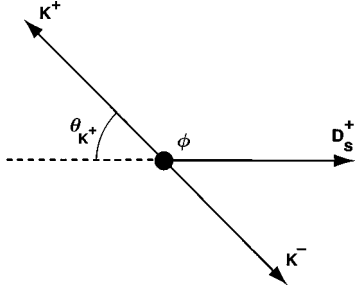


FIG. 2. Illustration of the helicity angle, θ_{K^+} . All vectors represent momenta in the ϕ rest frame.

$$(5) D_s^+ \rightarrow \eta' \pi^+, \eta' \rightarrow \eta \pi^+ \pi^-, \eta \rightarrow \pi^+ \pi^- \pi^0.$$

We require the pions that come directly from the weak decay to have momentum greater than $0.7 \text{ GeV}/c$ and the η or η' from the D_s^+ to have momentum greater than $1 \text{ GeV}/c$. This reduces the background from random combinations.

A. $D_s^+ \rightarrow \phi \pi^+$

Since this decay involves a pseudoscalar meson decaying into a vector meson and a pseudoscalar π^+ , the ϕ must be polarized in the helicity zero state. We take advantage of this by cutting on $\cos \theta_{K^+}$, where θ_{K^+} is the angle between the K^+ momentum and the direction opposite to the D_s^+ momentum in the ϕ rest frame. The angle is shown in Fig. 2. The signal has a $\cos^2 \theta_{K^+}$ distribution, while the background is flat in $\cos \theta_{K^+}$. We require $|\cos \theta_{K^+}| > 0.45$.

We select ϕ mesons within $\pm 8 \text{ MeV}$ of the peak mass, and form the $\phi \pi^+$ mass spectrum shown in Fig. 3. The $\phi \pi^+$ mass distribution shows two clear peaks, one from the D_s^+ and the other from the D^+ . To fit the spectrum we use four functions:

(1) The D_s^+ signal is fit to a sum of two Gaussians with a common mean; the widths and relative areas are fixed to values determined from the Monte Carlo signal simulation. The mean is allowed to vary in the fit.

(2) The D^+ signal shape is of the same form as for the D_s^+ , with the mass constrained to be $0.099 \text{ GeV}/c^2$ less than the D_s^+ mass, which is the precisely measured mass difference [10].

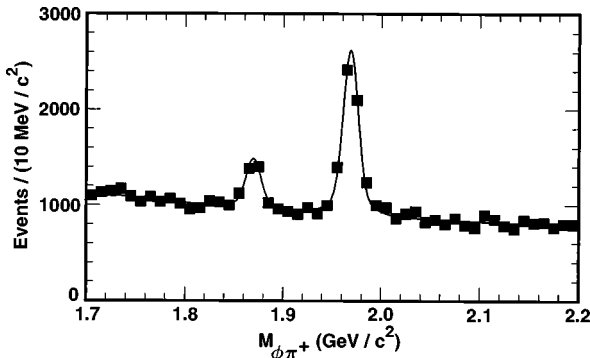


FIG. 3. The $M(\phi \pi^+)$ distribution. The larger peak is due to the decay $D_s^+ \rightarrow \phi \pi^+$; the smaller peak at lower mass is due to $D^+ \rightarrow \phi \pi^+$.

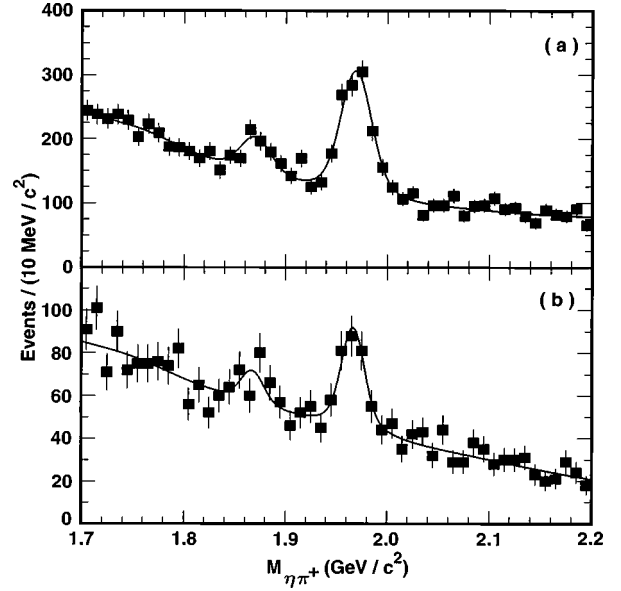


FIG. 4. The $M(\eta \pi^+)$ distribution for (a) $\eta \rightarrow \gamma \gamma$, (b) $\eta \rightarrow \pi^+ \pi^- \pi^0$.

(3) The shape of the function used to represent the $D_s^+ \rightarrow (\phi, \eta, \eta') \rho^+$ feedthrough is determined from Monte Carlo simulation. This feed through causes a broad peak in the mass of the $(\phi, \eta, \eta') \pi^+$ system centered at $1.7 \text{ GeV}/c^2$, which is parameterized with a Gaussian. The normalization of the feedthrough is determined from the measurement of the branching ratio [4].

(4) A second-order Chebyshev polynomial is used to represent the combinatoric background.

This fit yields 3748 ± 91 D_s^+ events. In all other fits, four functions are also used, although the combinatoric background shape depends on the particular mode.

B. $D_s^+ \rightarrow \eta \pi^+$

In Fig. 4 we show the $\eta \pi^+$ invariant mass spectrum for both decay modes of the η . The signal peaks are evident for both the D_s^+ and D^+ . The peak at the D_s^+ contains 766 ± 44 events for the channel $\eta \rightarrow \gamma \gamma$, and 154 ± 22 events for the channel $\eta \rightarrow \pi^+ \pi^- \pi^0$. Multiple entries into the plot from a single event are allowed, and no effort is made to select among them. The number of multiple entries is negligible for all decay modes discussed in this paper except for those using the $\eta \rightarrow \pi^+ \pi^- \pi^0$ decay. In Table I we list the

TABLE I. Fit results for $D_s^+ \rightarrow (\eta, \eta') \pi^+$. B is the branching ratio of the $\phi(\eta, \eta')$ decay mode that is used.

Mode	N	$\epsilon(\%)$	$\epsilon B(\%)$	$\Gamma/\Gamma(\phi \pi)$
$\phi \pi$	3748 ± 91	19.1 ± 0.2	9.4	
$\eta_{\gamma\gamma} \pi$	766 ± 44	9.6 ± 0.1	3.7	$0.52 \pm 0.03 \pm 0.04$
$\eta_{3\pi} \pi$	154 ± 22	4.5 ± 0.1	1.1	$0.35 \pm 0.05 \pm 0.06$
$\eta'(\eta_{\gamma\gamma}) \pi$	479 ± 26	6.7 ± 0.1	1.1	$1.09 \pm 0.06 \pm 0.07$
$\eta'(\eta_{3\pi}) \pi$	58 ± 9	1.9 ± 0.1	0.2	$0.73 \pm 0.11 \pm 0.12$

yields for different channels and their efficiencies for D_s^+ decay. We also list the measurement for the ratio $\Gamma(D_s^+ \rightarrow \eta_{\gamma\gamma}\pi^+)/\Gamma(D_s^+ \rightarrow \phi\pi^+)$. In the table ϵ is the efficiency and ϵB is the efficiency multiplied by the branching fraction of the secondary decays. The systematic errors for the efficiencies relative to the $\phi\pi^+$ mode have several sources and differ slightly from mode to mode. For the $\eta_{\gamma\gamma}\pi^+$ mode the systematic error includes uncertainties in the relative charged track (4%) and photon detection efficiencies (5%). We studied the Monte Carlo shape by letting the width of the two Gaussians vary in the fit and then calculated the shift in the central value, giving us an uncertainty of 3%. We also used different background shapes to determine the uncertainty due to the unknown background shape, and obtained an error of 4%. The total systematic error obtained by adding these uncorrelated errors in quadrature is 8%. For the $\eta_{3\pi}\pi^+$ mode the systematic error includes uncertainties in the photon detection efficiency (5%) and in the signal (5%) and background (8%) shapes. In addition there was a systematic error of (10%) due to the modeling of multiple entries. The fraction of all entries in the plot due to multiple entries is about 25%, and the 10% error quoted is an estimate of how well the multiple entries are simulated. The total systematic error obtained by adding these uncorrelated errors in quadrature is 15%.

The measured ratio for $\Gamma(D_s^+ \rightarrow \eta_{3\pi}\pi^+)/\Gamma(D_s^+ \rightarrow \phi\pi^+)$ shown in Table I is approximately two standard deviations lower than the corresponding ratio for the $\eta_{\gamma\gamma}$ mode, taking into account the systematic errors which are not in common to the two modes. The measurements of $D_s^+ \rightarrow \eta'\pi^+$, described in the next section, show a similar discrepancy, as do the $D^+ \rightarrow \eta\pi^+$ and $\eta'\pi^+$, although those have less statistical significance. As a result, we searched in some detail for a systematic discrepancy in reconstructing the two η decay modes. To calibrate the relative efficiency for these modes, and to check the reconstruction program, we studied events of the type $D^{*+} \rightarrow D^0\pi^+$ with $D^0 \rightarrow \bar{K}^{*0}\eta$. This has a very large and clean signal, and an η momentum spectrum very similar to that for the D_s^+ decays. Using this process, we measure $B(\eta \rightarrow \gamma\gamma)/B(\eta \rightarrow \pi^+\pi^-\pi^0) = 1.53 \pm 0.16 \pm 0.10$, compared to the Particle Data Group (PDG) value of 1.64 ± 0.04 [10]. This confirms that the relative efficiency for the two decay modes of the η is reproduced properly in the Monte Carlo simulation. Other checks using the data also reproduced the expected ratio of $B(\eta \rightarrow \gamma\gamma)/B(\eta \rightarrow \pi^+\pi^-\pi^0)$, although with limited statistical power. Since we were unable to isolate any systematic effect, we attribute the difference between the two $D_s^+ \rightarrow \eta\pi^+$ measurements to an unlikely set of statistical fluctuations.

The yields and relative branching ratios for all of the D^+ decays into the same final states are shown in Table II. The efficiencies for the D^+ modes are generally very close to those for the corresponding D_s^+ decays.

C. $D_s^+ \rightarrow \eta'\pi^+$

For this mode, we can apply cuts on both the η mass and the η' mass, reducing the background substantially. Each

TABLE II. Fit results for $D^+ \rightarrow (\eta, \eta')\pi^+$.

Mode	N	$\epsilon(\%)$	$\epsilon B(\%)$	$\Gamma/\Gamma(\phi\pi)$
$\phi\pi$	1133 ± 72	20.3 ± 0.2	9.9	
$\eta_{\gamma\gamma}\pi$	225 ± 38	9.6 ± 0.2	3.7	$0.53 \pm 0.09 \pm 0.05$
$\eta_{3\pi}\pi$	50 ± 20	4.6 ± 0.1	1.1	$0.40 \pm 0.15 \pm 0.07$
$\eta'(\eta_{\gamma\gamma})\pi$	114 ± 18	6.8 ± 0.1	1.1	$0.90 \pm 0.14 \pm 0.07$
$\eta'(\eta_{3\pi})\pi$	12 ± 7	1.9 ± 0.1	0.2	$0.52 \pm 0.29 \pm 0.09$

mass provides a kinematic constraint, helping to improve the resolution for the $\eta'\pi^+$ mass. As a result, these modes are significantly cleaner than $D_s^+ \rightarrow \eta\pi^+$. We require the momentum of the η' to be greater than 1.0 GeV/c.

In $D_s^+ \rightarrow \eta'\pi^+$, $\eta' \rightarrow \eta\pi^+\pi^-$, $\eta \rightarrow \pi^+\pi^-\pi^0$, we found that there are many events with multiple combinations of pions which satisfy our selection criteria. Most of them come from real η' decays in which different rearrangements of the same four charged pions (two directly from the η' and two from the η), plus the π^0 , pass our η and η' cuts. In these cases, the candidate has the proper $\eta'\pi^+$ mass even if these assignments are not all the correct ones. We take only one candidate per event, choosing the candidate with the minimum value of a χ^2 based on the π^0 , η , and η' masses: $\chi^2 = (\delta M_{\eta'})^2/\sigma_{\eta'}^2 + (\delta M_{\eta})^2/\sigma_{\eta}^2 + (\delta M_{\pi^0})^2/\sigma_{\pi^0}^2$.

In Fig. 5 we show the $\eta'\pi^+$ invariant mass spectrum for both η decay modes. The peak at the D_s^+ mass contains 479 ± 26 events for the channel $\eta \rightarrow \gamma\gamma$, and 58 ± 9 events for the channel $\eta \rightarrow \pi^+\pi^-\pi^0$. The efficiencies and relative branching ratios are shown in Table I. The systematic error on the branching ratio measurement due to the uncertainty in charged track efficiency is negligible for the case of $\eta \rightarrow \gamma\gamma$ because the final state has the same number of charged tracks as the normalizing mode. The main contributions to the systematic error are the uncertainties in the photon detec-

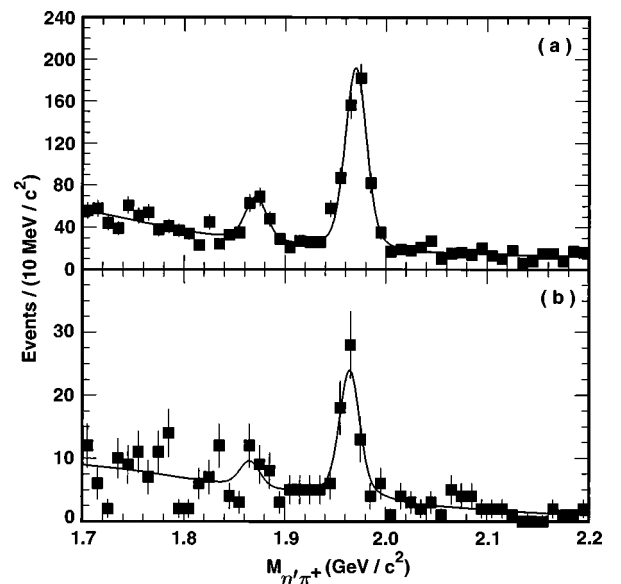
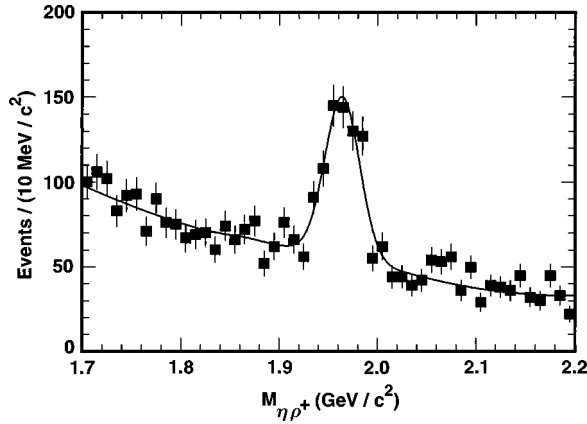


FIG. 5. The $M(\eta'\pi^+)$ distribution, using the decay mode $\eta' \rightarrow \eta\pi^+\pi^-$ with (a) $\eta \rightarrow \gamma\gamma$, (b) $\eta \rightarrow \pi^+\pi^-\pi^0$.

FIG. 6. The $M(\eta\rho^+)$ distribution, with $\eta \rightarrow \gamma\gamma$.

tion efficiency (5%) and in the shapes used to describe the signal (3%) and background (3%). The total systematic error obtained by adding these uncorrelated errors in quadrature is 6%. For the channel $\eta \rightarrow \pi^+\pi^-\pi^0$, the main contributions to the systematic error are the uncertainties in the efficiency for charged tracks (4%) and photons (5%) and in the shapes for the signal (10%) and background (4%), and in handling of events with multiple combinations (10%). The last error is a conservative estimate of how well the process of choosing the best candidate is simulated in the Monte Carlo calculation. The total systematic error obtained by adding these uncorrelated errors in quadrature is 16%. The resulting measurements are shown in Tables I and II.

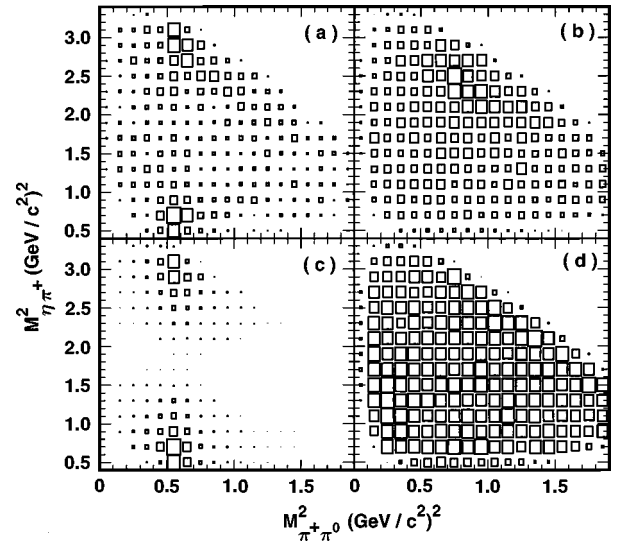
IV. D_s^+ DECAYS INTO MODES CONTAINING A ρ^+

The analogous D_s^+ decay channels, where the π^+ has been replaced by a ρ^+ , can be studied using very similar cuts. Because of lower rates, lower efficiency, and a serious problem with multiple combinations within the same event, the $\eta \rightarrow \pi^+\pi^-\pi^0$ decay does not add significantly to the measurements of these modes, and is not used. A data sample with about 20% less integrated luminosity was used for the measurements of these modes.

A. $D_s^+ \rightarrow \eta\rho^+$

For the decay mode $D_s^+ \rightarrow \eta\rho^+$, we need to consider the possibility of nonresonant $\eta\pi^+\pi^0$ feedthrough. For Fig. 6, we require the helicity angle to be in the range $|\cos\theta_{\pi^+}| > 0.45$, and the invariant mass of the $\pi^+\pi^0$ to be within $\pm 170 \text{ MeV}/c^2$ of the ρ^+ mass. A fit to the resulting $\eta\pi^+\pi^0$ mass spectrum is shown, yielding 589 ± 43 $D_s^+ \rightarrow \eta\rho^+$ candidates and 8 ± 32 $D^+ \rightarrow \eta\rho^+$ candidates; thus there is no evidence of $D^+ \rightarrow \eta\rho^+$. We cannot directly extract a branching ratio for $D_s^+ \rightarrow \eta\rho^+$, however, until we account for possible nonresonant feedthrough.

Although cuts on the helicity angle and on the ρ mass region can be used, the most reliable way to measure the resonant branching ratio is to fit the Dalitz plot. By doing this we make full use of the di-pion mass and the helicity angle to isolate the $\eta\rho^+$ signal. We therefore make a Dalitz plot of all events with $1.94 < M(\eta\pi^+\pi^0) < 1.99 \text{ GeV}/c^2$, re-

FIG. 7. Dalitz plot of $D_s^+ \rightarrow \eta\rho^+$, with $\eta \rightarrow \gamma\gamma$. The horizontal axis is $M_{\pi^+\pi^0}^2$; the vertical axis is $M_{\eta\pi^+}^2$. (a) Data signal region; (b) data M_{D_s} sidebands; (c) MC signal; (d) MC simulation of nonresonant $\eta\pi^+\pi^0$, generated according to phase space.

moving the cuts on the helicity angle and on the $\pi^+\pi^0$ mass. In Fig. 7 we show four Dalitz plots: (a) the signal region in the data, defined as $1.94 < M(\eta\pi^+\pi^0) < 1.99 \text{ GeV}/c^2$; (b) the M_{D_s} data sidebands, which are the mass regions $1.75 < M(\eta\pi^+\pi^0) < 1.90 \text{ GeV}/c^2$ and $2.04 < M(\eta\pi^+\pi^0) < 2.24 \text{ GeV}/c^2$; (c) the full Monte Carlo data of the $\eta\rho^+$ signal; and (d) a simulation using a parametrized Monte Carlo data of nonresonant $\eta\pi^+\pi^0$ events generated according to phase space.

We do not expect $\eta\pi$ resonant structures in this Dalitz plot because isospin forbids $s\bar{s} \rightarrow \eta\pi$. For all four Dalitz plots, we recalculate the values of $M^2(\eta\pi^+)$ and $M^2(\pi^+\pi^0)$ so that the Dalitz boundary corresponds exactly to that of the mass of the D_s^+ [10], giving the sidebands the same boundary as the signal region. This causes negligible smearing of the ρ^+ resonance.

The most obvious feature of the Dalitz plot is that the ρ^+ region stands out so clearly in the data, even though there is a significant non- D_s^+ background which contains very little ρ^+ . A binned Dalitz fit to the data distribution in the signal region was performed using the sum of the distributions in the other three plots in Fig. 7. The normalization of the non- D_s^+ component is fixed using a fit to the $\eta\rho^+$ mass distribution as in Fig. 6 but without helicity angle and ρ mass cuts. The number of resonant and nonresonant D_s^+ events is varied in the fit, with no interference term allowed. The results of the fit are shown in Table III. The systematic error includes uncertainties in the efficiencies for charged tracks (4%) and photons (10%) and the shapes for the signal (4%) and the background (3%).

As can be seen from Fig. 7, any nonresonant $\eta\pi^+\pi^0$ signal is not easily distinguishable from background in the Dalitz plot. A total of $99 \pm 41 \pm 40$ nonresonant events are seen from the fit. Since this is not significant enough to measure the branching ratio, we use it to determine the upper

TABLE III. Fit results for $D_s^+ \rightarrow (\eta, \eta') \rho^+$.

Mode	N	$\epsilon(\%)$	$\epsilon B(\%)$	$\Gamma/\Gamma(\phi\pi)$
$\phi\pi^+$	300 ± 81	19.1 ± 0.2	9.4	
$\eta\rho^+$	447 ± 31	1.82 ± 0.07	0.47	$2.98 \pm 0.20 \pm 0.39$
$\eta'\rho^+$	137 ± 14	1.36 ± 0.04	0.15	$2.78 \pm 0.28 \pm 0.30$

limit $\Gamma(D_s^+ \rightarrow \eta\pi^+\pi^0)/\Gamma(D_s^+ \rightarrow \phi\pi^+) < 1.1$ at the 90% confidence level.

In order to understand the systematic error due to possible interference between the resonant and nonresonant decays we also did a coherent Dalitz fit. The density of the events in the Dalitz plot is represented by the expression

$$I = A_1^2 + A_2^2 + B \times 2A_1A_2\cos(\delta_1 - \delta_2),$$

where A_1 and δ_1 are the amplitude and phase of the Breit-Wigner resonance, A_2 and δ_2 are the amplitude and phase of the nonresonant decay, both of which are assumed to be constant, and B is an additional constant which is allowed to vary from zero to one. The case $B=0$ corresponds to no interference between the resonant and nonresonant parts; the case $B=1$ corresponds to full interference, expected if the nonresonant case were indeed a single partial wave with constant phase. The true case could lie anywhere between these two limits. In the fit when the constant B is allowed to float it takes the value 0.24 ± 0.20 , consistent with no interference. We therefore use the result from the incoherent fit to determine the branching ratio, and use the result from the coherent fit with $B=0.44$ to find a conservative systematic error from this source. This corresponds to a 3.6% error. The total systematic error, obtained by adding this error in quadrature with the other systematic errors mentioned above, is estimated to be 12%.

B. $D_s^+ \rightarrow \eta' \rho^+$

The decay $D_s^+ \rightarrow \eta' \rho^+$ was reconstructed using the decay mode $\eta' \rightarrow \eta\pi^+\pi^-$, with $\eta \rightarrow \gamma\gamma$. We require the momentum of the η' to be greater than 1.0 GeV/c and the invariant mass of the two pions to be within ± 170 MeV of the ρ^+ mass. In Fig. 8 we can see a clear peak of $M_{\eta'\pi^+\pi^0}$. The fit

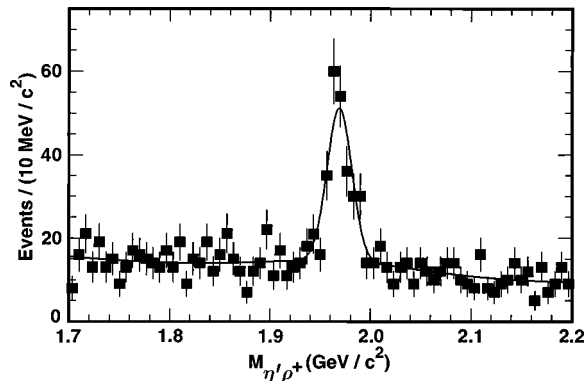


FIG. 8. The $M(\eta' \rho^+)$ distribution, with $\eta' \rightarrow \eta\pi^+\pi^-$, $\eta \rightarrow \gamma\gamma$.

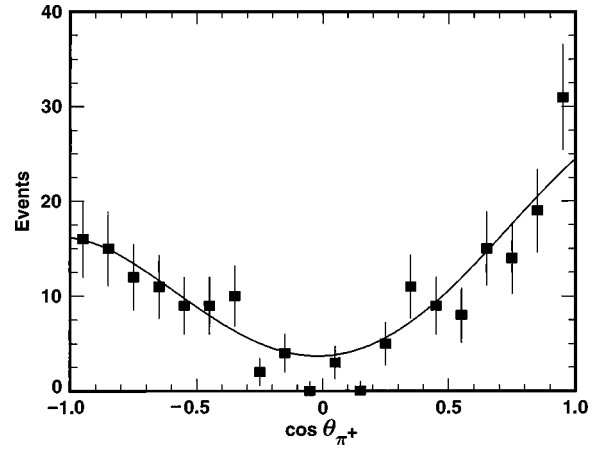


FIG. 9. The helicity angle distribution for events in the D_s^+ mass peak for the decay channel $D_s^+ \rightarrow \eta' \rho^+$.

yields 181 ± 18 $D_s^+ \rightarrow \eta' \rho^+$ events and -4 ± 10 $D^+ \rightarrow \eta' \rho^+$ events; thus there is no evidence for $D^+ \rightarrow \eta' \rho^+$.

As for the case of the $\eta\rho^+$ decay mode, we need to subtract any nonresonant feedthrough into the $\eta' \rho^+$ final state. In this case, however, a Dalitz plot is not as useful in separating the signal from background, because the kinematic range for the di-pion mass does not extend beyond the region of the ρ . We do not expect $\eta'\pi$ resonant structures in this Dalitz plot because isospin forbids $s\bar{s} \rightarrow \eta'\pi$. We therefore fit the angular distribution alone to extract the ρ component. As for the case of the Dalitz fit for $\eta\rho^+$, we use three components in the fit: (a) the resonant signal shape, a fourth-order polynomial determined from the Monte Carlo, simulation which includes the distortion of the pure $\cos^2 \theta_{\pi^+}$ shape due to detector acceptance; (b) a nonresonant D_s^+ shape, which is linear; and (c) a non- D_s^+ background shape, which is a first-order polynomial determined by fitting the sidebands. As in the Dalitz fit, we fix the background normalization from the D_s^+ mass fit, and vary the normalizations of the signal and nonresonant parts.

Figure 9 shows the fit of the helicity angle distribution for the events in the D_s^+ mass peak. The results of the fit are shown in Table III. The total systematic error of 11% includes uncertainties in the photon detection efficiency (10%) and in the signal (4%), background (3%), and nonresonant (2%) shapes. The best fit has no nonresonant $D_s^+ \rightarrow \eta' \pi^+\pi^0$ events, with an upper limit of 15 events. Converting this to an upper limit, taking into account similar systematic errors as for the resonance mode, we find that $\Gamma(D_s^+ \rightarrow \eta' \pi^+\pi^0)/\Gamma(D_s^+ \rightarrow \phi\pi^+) < 0.4$ at the 90% confidence level.

TABLE IV. Fit results for $D^+ \rightarrow (\eta, \eta') \rho^+$.

Type	N	$\epsilon(\%)$	$\epsilon B(\%)$	$\Gamma/\Gamma(\phi\pi)(90\% C.L.)$
$\phi\pi^+$	970 ± 65	20.3 ± 0.2	9.9	
$\eta\rho^+$	8 ± 32	2.1 ± 0.1	0.55	< 1.11
$\eta'\rho^+$	-4 ± 10	1.7 ± 0.1	0.19	< 0.86

TABLE V. Measurements and predictions for branching ratios of D_s^+ decays.

Mode	$\Gamma/\Gamma(\phi\pi^+)$	BSW [11]	HK [5]	BLP [6]
$\eta\pi$	0.48 ± 0.05	1.04	0.58 ± 0.15	0.30
$\eta\rho$	2.98 ± 0.44	1.96	2.86 ± 0.71	1.83
$\eta'\pi$	1.03 ± 0.09	0.61	1.55 ± 0.42	1.32
$\eta'\rho$	2.78 ± 0.41	0.55	$0.43^{+0.55}_{-0.32}$	0.59

The yields and upper limits on the branching ratios for the D^+ decays into final states with a ρ^+ are shown in Table IV.

V. CONCLUSIONS

We have measured with improved statistics the branching ratios of the two-body hadronic decays of the D_s^+ : $D_s^+ \rightarrow \eta\pi^+$, $\eta'\pi^+$, $\eta\rho^+$, and $\eta'\rho^+$. The results are consistent with the previous CLEO measurements [4] and have improved errors. Using weighted averages of the two η modes, our results for $D_s^+ \rightarrow (\eta, \eta')\pi^+$ are

$$\frac{\Gamma(D_s^+ \rightarrow \eta\pi^+)}{\Gamma(D_s^+ \rightarrow \phi\pi^+)} = 0.48 \pm 0.03 \pm 0.04$$

and

$$\frac{\Gamma(D_s^+ \rightarrow \eta'\pi^+)}{\Gamma(D_s^+ \rightarrow \phi\pi^+)} = 1.03 \pm 0.06 \pm 0.07.$$

The results for the ρ modes are

$$\frac{\Gamma(D_s^+ \rightarrow \eta\rho^+)}{\Gamma(D_s^+ \rightarrow \phi\pi^+)} = 2.98 \pm 0.20 \pm 0.39$$

and

$$\frac{\Gamma(D_s^+ \rightarrow \eta'\rho^+)}{\Gamma(D_s^+ \rightarrow \phi\pi^+)} = 2.78 \pm 0.28 \pm 0.30.$$

These measurements have statistical errors typically a factor of 2 smaller than the previous CLEO results [4] and the systematic errors are smaller by about a factor of 1.5.

Using these measurements and the published CLEO semi-leptonic measurements [7], we can calculate the ratios which test factorization: $\Gamma(D_s^+ \rightarrow \eta\rho^+)/\Gamma(D_s^+ \rightarrow \eta e^+ \nu_e) = 4.4 \pm 1.2$ and $\Gamma(D_s^+ \rightarrow \eta'\rho^+)/\Gamma(D_s^+ \rightarrow \eta' e^+ \nu_e) = 12.0 \pm 4.3$. The branching ratio for the mode $D_s^+ \rightarrow \eta'\rho^+$ is much larger than the value of 2.9 expected from factorization. Using the normalization $B(D_s^+ \rightarrow \phi\pi^+) = (3.6 \pm 0.9)\%$ [10], we calcu-

TABLE VI. Measurements and predictions for branching fractions of D^+ decays. The experimental upper limits are at the 90% confidence level.

Mode	Branching fraction (%)	BSW [11]	HK [5]	BLP [6]
$\eta\pi$	0.30 ± 0.06	0.004	0.68 ± 0.21	0.34
$\eta\rho$	< 0.68	0.06	< 0.48	0.01
$\eta'\pi$	0.50 ± 0.10	0.16	< 0.48	0.73
$\eta'\rho$	< 0.52	0.05	< 0.07	0.12

late $B(D_s^+ \rightarrow \eta'\rho^+) = (10.0 \pm 1.5 \pm 2.5)\%$, where the second error is due to the uncertainty in the $D_s^+ \rightarrow \phi\pi^+$ branching fraction. This branching fraction is very large, considering that the flavor wave function of the η' is only partly $s\bar{s}$ and that the rate is suppressed for such a P -wave decay very close to threshold. There is no obvious mechanism by which final state interactions could cause such a large enhancement of one of the dominant decay modes.

Table V summarizes the measurements of branching ratios for all four D_s^+ decays and compares them with theoretical calculations. Models which are successful in predicting other charm hadronic modes reasonably well predict $B(D_s^+ \rightarrow \eta'\rho^+)$ to be 1–3% [5,6,11]. This failure leads theorists to consider contributions to the amplitude from decay diagrams other than that shown in Fig. 1. For example, Ball *et al.* [12] argue that the high branching ratio for $D_s^+ \rightarrow \eta'\rho$ could be due to a $c\bar{s}$ annihilation into a W^+ and two gluons, in which the two gluons hadronize as an η' .

Using the normalization $B(D^+ \rightarrow \phi\pi^+) = (6.1 \pm 0.6) \times 10^{-3}$ [10], we also calculate the D^+ branching fractions to the same final states. Table VI summarizes the results. Since the D^+ decays involve two diagrams which interfere, the theoretical calculations vary widely, and are expected to be somewhat less reliable than for the D_s^+ case.

ACKNOWLEDGMENTS

We gratefully acknowledge the effort of the CESR staff in providing us with excellent luminosity and running conditions. J.P.A., J.R.P., and I.P.J.S. thank the NYI program of the NSF, M.S. thanks the PFF program of the NSF, G.E. thanks the Heisenberg Foundation, K.K.G., M.S., H.N.N., T.S., and H.Y. thank the OJI program of the DOE, J.R.P., K.H., M.S. and V.S. thank the A.P. Sloan Foundation, R.W. thanks the Alexander von Humboldt Stiftung, and M.S. thanks Research Corporation for support. This work was supported by the National Science Foundation, the U.S. Department of Energy, and the Natural Sciences and Engineering Research Council of Canada.

- [1] A. N. Kamal, Q. P. Xu, and A. Czarnecki, Phys. Rev. D **49**, 1330 (1994).
[2] CLEO Collaboration, A. Bean *et al.*, Phys. Lett. B **317**, 647 (1993).

- [3] Note that the approximate equality of the two ratios is coincidental. See [1].
[4] CLEO Collaboration, M. Daoudi *et al.*, Phys. Rev. D **45**, 3965 (1992). The branching ratios measured in that paper were

$\Gamma(D_s^+ \rightarrow \eta \pi^+)/\Gamma(D_s^+ \rightarrow \phi \pi^+) = 0.54 \pm 0.09 \pm 0.06$, $\Gamma(D_s^+ \rightarrow \eta' \pi^+)/\Gamma(D_s^+ \rightarrow \phi \pi^+) = 1.20 \pm 0.15 \pm 0.11$,
 $\Gamma(D_s^+ \rightarrow \eta \rho^+)/\Gamma(D_s^+ \rightarrow \phi \pi^+) = 2.86 \pm 0.38^{+0.36}_{-0.38}$, and $\Gamma(D_s^+ \rightarrow \eta' \rho^+)/\Gamma(D_s^+ \rightarrow \phi \pi^+) = 3.44 \pm 0.62^{+0.44}_{-0.46}$. The present paper includes the data used in the 1992 paper. Thus the new results should not be averaged with the old results.

- [5] I. Hinchliffe and T. A. Kaeding, Phys. Rev. D **54**, 914 (1996).
- [6] F. Buccella, M. Lusignoli, and A. Pugliese, Phys. Lett. B **379**, 24 (1996).
- [7] CLEO Collaboration, G. Brandenburg *et al.*, Phys. Rev. Lett.

75, 3804 (1995).

- [8] CLEO Collaboration, Y. Kubota *et al.*, Nucl. Instrum. Methods Phys. Res. A **320**, 66 (1992).
- [9] R. Brun *et al.*, Computer Code GEANT3, Report No. CERN DD/EE/84-1, 1987.
- [10] Particle Data Group, R. M. Barnett *et al.*, Phys. Rev. D **54**, 1 (1996).
- [11] M. Bauer, B. Stech, and M. Wirbel, Z. Phys. C **34**, 103 (1987).
- [12] P. Ball, J. M. Frere, and M. Tytgat, Phys. Lett. B **365**, 367 (1996).